

---

---

# Lung Dose Measured on Postradioembolization $^{90}\text{Y}$ PET/CT and Incidence of Radiation Pneumonitis

Martina Stella, Rob van Rooij, Marnix G.E.H. Lam, Hugo W.A.M. de Jong, and Arthur J.A.T. Braat

*Division of Imaging and Oncology, University Medical Center Utrecht, Utrecht University, Utrecht, The Netherlands*

Radiation pneumonitis is a rare but possibly fatal side effect of  $^{90}\text{Y}$  radioembolization. It may occur 1–6 mo after therapy, if a significant part of the  $^{90}\text{Y}$  microspheres shunts to the lungs. In current clinical practice, a predicted lung dose greater than 30 Gy is considered a criterion to exclude patients from treatment. However, contrasting findings regarding the occurrence of radiation pneumonitis and lung dose were previously reported in the literature. In this study, the relationship between the lung dose and the eventual occurrence of radiation pneumonitis after  $^{90}\text{Y}$  radioembolization was investigated. **Methods:** We retrospectively analyzed 317  $^{90}\text{Y}$  liver radioembolization procedures performed during an 8-y period (February 2012 to September 2020). We calculated the predicted lung mean dose (LMD) using  $^{99\text{m}}\text{Tc}$ -MAA planar scintigraphy ( $\text{LMD}_{\text{MAA}}$ ) acquired during the planning phase and left LMD ( $\text{LMD}_{\text{Y-90}}$ ) using the  $^{90}\text{Y}$  PET/CT acquired after the treatment. For the lung dose computation, we used the left lung as the representative lung volume, to compensate for scatter from the liver moving in the craniocaudal direction because of breathing and mainly affecting the right lung. **Results:** In total, 272 patients underwent  $^{90}\text{Y}$  procedures, of which 63% were performed with glass microspheres and 37% with resin microspheres. The median injected activity was 1,974 MBq (range, 242–9,538 MBq). The median  $\text{LMD}_{\text{MAA}}$  was 3.5 Gy (range, 0.2–89.0 Gy). For 14 procedures,  $\text{LMD}_{\text{MAA}}$  was more than 30 Gy. Median  $\text{LMD}_{\text{Y-90}}$  was 1 Gy (range, 0.0–22.1 Gy). No patients had an  $\text{LMD}_{\text{Y-90}}$  of more than 30 Gy. Of the 3 patients with an  $\text{LMD}_{\text{Y-90}}$  of more than 12 Gy, 2 patients (one with an  $\text{LMD}_{\text{Y-90}}$  of 22.1 Gy and an  $\text{LMD}_{\text{MAA}}$  of 89 Gy; the other with an  $\text{LMD}_{\text{Y-90}}$  of 17.7 Gy and an  $\text{LMD}_{\text{MAA}}$  of 34.1 Gy) developed radiation pneumonitis and consequently died. The third patient, with an  $\text{LMD}_{\text{Y-90}}$  of 18.4 Gy ( $\text{LMD}_{\text{MAA}}$ , 29.1 Gy), died 2 mo after treatment, before the imaging evaluation, because of progressive disease. **Conclusion:** The occurrence of radiation pneumonitis as a consequence of a lung shunt after  $^{90}\text{Y}$  radioembolization is rare (<1%). No radiation pneumonitis developed in patients with a measured  $\text{LMD}_{\text{Y-90}}$  lower than 12 Gy.

**Key Words:**  $^{90}\text{Y}$  radioembolization; lung-dose; radiation pneumonitis;  $^{90}\text{Y}$  PET dosimetry;  $^{99\text{m}}\text{Tc}$ -MAA lung dose predicted

**J Nucl Med 2022; 63:1075–1080**

DOI: 10.2967/jnumed.121.263143

---

**R**adioembolization is a well-established treatment for primary and metastatic liver malignancies (1). It is defined as percutaneous, transarterial injection (2) of embolic particles (diameter, 20–60  $\mu\text{m}$ ) loaded with  $^{90}\text{Y}$  or  $^{166}\text{Ho}$ . Because hepatic tumors are

preferentially fed by the blood supply from the hepatic artery, radioembolization preferentially deposits radioactive microspheres in the peritumoral and intratumoral arterial vasculature through the hepatic artery, relatively sparing normal liver parenchyma (3). Three devices are commercially available: glass  $^{90}\text{Y}$  microspheres (TheraSphere; Boston Scientific Corp.), resin  $^{90}\text{Y}$  microspheres (SIR-spheres; SIRTech Medical Limited), and poly-L-lactic acid  $^{166}\text{Ho}$  microspheres (QuiremSpheres; Quirem BV). If a significant number of microspheres pass through tumor-associated arteriovenous shunts and lodge in the pulmonary vasculature, a dose-dependent radiation-induced pneumonitis may ensue. Therefore, the presence of significant hepatopulmonary shunting is a relative contraindication for radioembolization. The current approach to radioembolization with respect to radiation pneumonitis is driven mainly by 2 seminal publications (4,5) that have strongly influenced the guidance on lung dose limits after radioembolization. On the basis of clinical evidence from these studies, a lung dose limit of 30 Gy was recommended for a single radioembolization treatment (6) and adopted in the instruction manuals for these devices. For this reason, assessment of the lung shunt fraction (LSF), which is a prediction of the eventual lung mean dose (LMD) after the radioembolization treatment, is paramount before administration of the radioactive particles.

For  $^{90}\text{Y}$ , this prediction is performed using  $^{99\text{m}}\text{Tc}$ -macroaggregated albumin (MAA). Despite being the current clinical practice,  $^{99\text{m}}\text{Tc}$ -MAA planar scintigraphy is poor in predicting the dose to the lungs, especially when computing the LSF ( $\text{LSF}_{\text{MAA}}$ ) and, consequently, the predicted lung mean dose ( $\text{LMD}_{\text{MAA}}$ ). SPECT/CT imaging can improve the LSF computation (7). However, discrepancies between  $^{90}\text{Y}$  and  $^{99\text{m}}\text{Tc}$ -MAA particles reduce the predictive value (8,9).

The aim of this study was to assess the occurrence of radiation pneumonitis after  $^{90}\text{Y}$  liver radioembolization and perform lung dosimetry on  $^{90}\text{Y}$  PET/CT to evaluate the currently assumed lung dose restriction of less than 30 Gy. Although multiple studies on lung dose after  $^{90}\text{Y}$  radioembolization have been reported, they all focus on the  $^{99\text{m}}\text{Tc}$ -MAA-based lung dose estimate during the pretreatment phase. Conversely, this study retrospectively quantified the actual dose received by the lungs after  $^{90}\text{Y}$  radioembolization, exploiting the potential of posttreatment PET/CT (10) and accurate  $^{90}\text{Y}$  dosimetry (11). Knowledge of the actual dose would provide a better insight into the lung dose after  $^{90}\text{Y}$  radioembolization and the related occurrence of radiation pneumonitis.

## MATERIALS AND METHODS

This single-center, retrospective analysis of all patients treated with  $^{90}\text{Y}$  radioembolization between February 2012 and September 2020 was approved by the ethical research committee, and the need for

Received Sep. 1, 2021; revision accepted Oct. 26, 2021.

For correspondence or reprints, contact Martina Stella (m.stella@umcutrecht.nl).

Published online Nov. 12, 2021.

COPYRIGHT © 2022 by the Society of Nuclear Medicine and Molecular Imaging.

informed consent was waived. Before radioembolization treatment, patient eligibility for treatment was assessed by a  $^{99m}\text{Tc}$ -MAA injection in the hepatic artery, to assess the intrahepatic distribution and potential extrahepatic deposition of activity (including lung shunting). After the injection, planar  $\gamma$ -camera scintigraphy (to compute  $\text{LSF}_{\text{MAA}}$ ) and SPECT/CT (to visually assess extrahepatic depositions) were performed. To assess the treatment outcome, posttreatment  $^{90}\text{Y}$  PET/CT was performed on the same day as, or the day after, treatment. LMD after  $^{90}\text{Y}$  radioembolization was assessed using the posttreatment  $^{90}\text{Y}$  PET/CT.

### $^{90}\text{Y}$ PET/CT Protocol

Images were acquired on a Biograph mCT or Biograph Vision 600 time-of-flight PET/CT scanner (Siemens Medical Solutions), with 40- and 64-slice CT scanners, respectively. The images were reconstructed using an iterative algorithm including model-based scatter correction, which encompasses a point-spread-function model of the detector response together with time-of-flight information. To correct for attenuation, a low-dose CT scan acquired right after the PET scan was used. Both PET scanners and the reconstruction protocol were validated for  $^{90}\text{Y}$  quantitative imaging (12).

### $^{99m}\text{Tc}$ -MAA-Based LMD Predicted

To determine each patient's eligibility,  $\text{LMD}_{\text{MAA}}$  was calculated as follows:

$$\text{LMD}_{\text{MAA}} = \frac{\text{activity}_{\text{prescribed}}(\text{GBq}) \times \text{LSF}_{\text{MAA}} \times 50(\text{Gy} \times \text{kg}/\text{GBq})}{\text{lung mass}(\text{kg})},$$

where lung mass is assumed to be 1 kg and  $50[\text{Gy} \times \text{kg}/\text{GBq}]$  is the standard conversion factor for  $^{90}\text{Y}$ .  $\text{LSF}_{\text{MAA}}$  was computed as follows:

$$\text{LSF}_{\text{MAA}} = \frac{\text{count}_{\text{lungs}}}{\text{count}_{\text{lungs}} + \text{count}_{\text{liver}}} \times 100\%.$$

The counts were computed using the geometric mean following standard clinical practice (13). Lungs and liver were delineated on the planar scintigrams by the imaging technicians.

### $^{90}\text{Y}$ PET-Based LMD

To assess the LMD after treatment, lungs masks were automatically segmented on the CT scans corresponding to the PET scans used for dosimetric purposes, applying a freely available U-net that extracts the right and left lungs separately (14). All masks were visually checked to ensure correct segmentation. Since the right lung was affected by scatter from the liver moving in the craniocaudal direction because of breathing (Fig. 1), only the left lung was considered as representative for computation of the LMD. The  $^{90}\text{Y}$  PET-based left LMD ( $\text{LMD}_{\text{Y-90}}$ ) was computed as follows:

$$\text{LMD}_{\text{Y-90}} = \frac{\text{mean activity concentration}_{\text{left lung}} \left( \frac{\text{Bq}}{\text{mL}} \right) \times 5 \times 10^{-8}(\text{J} \times \text{s})}{\text{lung density}(\text{kg}/\text{cm}^3)}.$$

The mean activity concentration in the left lung volume of interest (measured in Bq/mL) was computed as the mean of the voxel value (Bq/mL) within the left lung mask. Lung density was assumed to be  $2.6 \times 10^{-4}(\text{kg}/\text{mm}^3)$  (15), whereas  $5 \times 10^{-8}(\text{J} \times \text{s})$  represents the deposited energy due to  $\beta$ -decay of 1 Bq of injected  $^{90}\text{Y}$  activity (16). The mean activity concentration was corrected for  $^{90}\text{Y}$  decay considering the time difference between the activity administration and the scanning. Three commonly applied assumptions were adapted for this study. First, the maximal range for  $^{90}\text{Y}$   $\beta$ -particles in tissue is 1.2 cm, which is on the same order of magnitude as the resolution of  $^{90}\text{Y}$  PET; thus, it is assumed that the total energy is deposited within the voxel

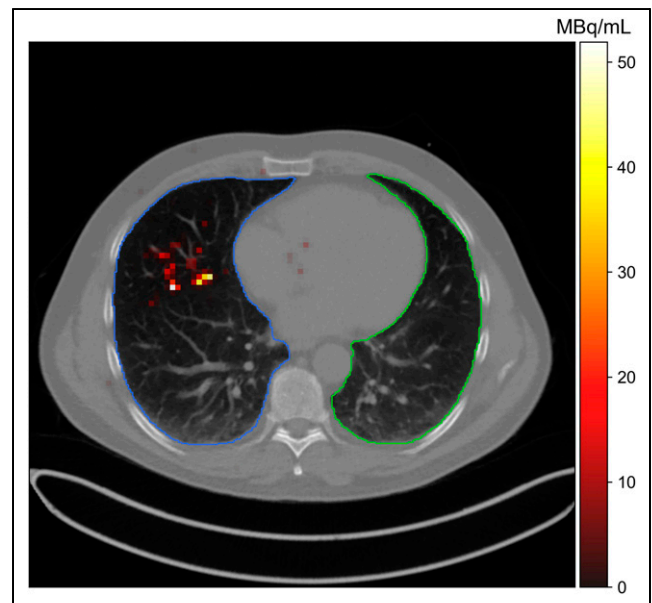


**FIGURE 1.** Posttreatment  $^{90}\text{Y}$  PET/CT scan of 47-year-old man diagnosed with colorectal cancer. LMD considering both lobes was 61 Gy.  $^{90}\text{Y}$  PET image shows activity in right lung (blue contour) due to liver motion in craniocaudal direction and rim field-of-view artifact and leading to right LMD of 100 Gy, which was main contributor to LMD. Left LMD (computed within green contour) was 3 Gy.

of origin (17). Second,  $^{90}\text{Y}$  distributes uniformly in cases of lung shunting. Third, lung density is the same for all patients.

### $^{90}\text{Y}$ PET-Based LSF

Because  $\text{LSF}_{\text{MAA}}$  is a poor predictor for actual lung shunting, in this work LSF measured using  $^{90}\text{Y}$  PET/CT ( $\text{LSF}_{\text{Y-90}}$ ) was computed as a metric to evaluate differences among tumor type.  $\text{LSF}_{\text{Y-90}}$  was defined as the ratio between the activity in the lungs and the total activity administered, as follows:

$$\text{LSF}_{\text{Y-90}} = \frac{\text{mean activity concentration}_{\text{lungs}} \left( \frac{\text{Bq}}{\text{mL}} \right) \times \text{lung volume}(\text{mL})}{\text{activity}_{\text{prescribed}}(\text{Bq})} \times 100\%.$$

As was done for  $\text{LMD}_{\text{Y-90}}$ , the mean activity concentration in the lungs was computed as the mean of the voxel value (Bq/mL) within both lung masks. Lung volume was assumed to be the same among all subjects, considering a lung mass of 1 kg and a lung density of  $2.6 \times 10^{-4}(\text{kg}/\text{mL})$ , previously assumed.

### Statistical Analysis

The statistical variables under investigation to characterize radiation pneumonitis were  $\text{LMD}_{\text{MAA}}$  and  $\text{LMD}_{\text{Y-90}}$ . When assessing the eventual difference among tumor types or, in the case of hepatocellular carcinoma (HCC) patients, between the presence and absence of portal hypertension and thrombus, we considered  $\text{LSF}_{\text{Y-90}}$  in order to take into account the difference in delivered activity. The normality of distribution was assessed visually and by a Q-Q plot. If variables were not normally distributed, nonparametric tests were used for further analysis.

The Mann-Whitney  $U$  test with an  $\alpha$ -significance level of 0.05 was used for HCC patients to assess whether the occurrence of thrombus or portal hypertension caused a statistically significant difference in left LMD.

The Kruskal–Wallis H test with an  $\alpha$ -significance level of 0.05 was used to determine whether statistical differences existed between different tumor types.

## RESULTS

### Patient Population

Patients and treatment characteristics are summarized in Table 1. The institutional review board approved this retrospective study and waived the need for informed consent. There were 170 men and 102 women, who underwent a total of 317  $^{90}\text{Y}$  radioembolization procedures (mean number of procedures per patient, 1.17; range, 1–5). Most patients were treated for liver metastases of various origins, whereas 25% had HCC. Glass microspheres were used for 200 treatments, and the remaining 117 procedures were performed with resin microspheres. The median administered activity per procedure was 2,278 MBq (range, 277–9,636 MBq) and 1,877 MBq (range, 516–3,245 MBq) for glass and resin microspheres, respectively. The median volume within the PET field of view was 1,713 mL (392–7,851 mL) and 733 mL (range, 80–3,792 mL) for both lungs and the left lung, respectively.

### Data Analysis

The median  $\text{LMD}_{\text{MAA}}$  was 3.5 Gy (range, 0.2–89.0 Gy). For 14 patients,  $\text{LMD}_{\text{MAA}}$  was greater than 30 Gy, above which  $^{90}\text{Y}$  radioembolization is contraindicated (18). Nonetheless, after clinical consideration by the treating physicians, these patients did undergo  $^{90}\text{Y}$  radioembolization treatment.

The median posttreatment  $\text{LMD}_{\text{Y-90}}$  was 1.0 Gy (range, 0.0–22.1 Gy), with 3 cases above 12 Gy. No cases of  $\text{LMD}_{\text{Y-90}}$  above 30 Gy were reported.

The median  $\text{LSF}_{\text{Y-90}}$  was 4.13% (range, 0.27%–39.02%). Overall, according to the Kruskal–Wallis H test, no statistically significant difference existed among tumor types ( $P = 0.1$ ). However, pairwise comparison among tumor types returned a statistically significant difference between patients with neuroendocrine tumor and patients with colorectal cancer, HCC, or other conditions, with  $P$  values of 0.008, 0.010, and 0.022, respectively. Statistically significant  $P$  values for  $\text{LSF}_{\text{Y-90}}$  from the pairwise comparison among tumor types are reported in Table 2. A box plot depicting the  $\text{LSF}_{\text{Y-90}}$  per tumor type is shown in Figure 2.

$\text{LMD}_{\text{Y-90}}$  as a function of  $\text{LMD}_{\text{MAA}}$  is reported in Figure 3. The data suggest that radiation pneumonitis did not occur among subjects with an  $\text{LMD}_{\text{Y-90}}$  below 12 Gy. On the basis of this empiric value and the 30-Gy limit for  $\text{LMD}_{\text{MAA}}$ , the number of true-negative, true-positive, false-negative, and false-positive cases is reported in Figure 3.

### Radiation Pneumonitis

Radiation pneumonitis did not occur in any subject with an  $\text{LMD}_{\text{Y-90}}$  below 12 Gy. Radiation pneumonitis occurred in 2 patients, both of whom were diagnosed with HCC and treated with glass microspheres. The first patient had the highest  $\text{LMD}_{\text{Y-90}}$  (22.1 Gy) of all subjects. This patient had no thrombus or portal hypertension. During the pretreatment work-up,  $\text{LMD}_{\text{MAA}}$  was 89.0 Gy ( $\text{LSF}_{\text{MAA}}$ , 23%), and SPECT/CT showed no evidence of extrahepatic depositions in the upper abdomen. The total administered activity was 7,775 MBq. The second patient had an  $\text{LMD}_{\text{Y-90}}$  of 17.7 Gy in the presence of both portal vein tumor thrombosis and portal hypertension.  $\text{LMD}_{\text{MAA}}$  was 34.1 Gy ( $\text{LSF}_{\text{MAA}}$ , 50%), and SPECT/CT showed no evidence of extrahepatic depositions in the upper abdomen. The total administered activity was

**TABLE 1**  
Baseline and Treatment Characteristics

Characteristic	Data
Patients	272
Procedures	317
Sex	
Male	170 (62.5%)
Female	102 (37.5%)
Mean age	64.56 (17–90)
Sphere type	
Glass	200 (63%)
Resin	117 (37%)
Median administered activity (MBq)	
Glass	2,278 (277–9,636)
Resin	1,877 (516–3,245)
Mean number of $^{90}\text{Y}$ sessions	1.17 (1–5)
Tumor types	
Colorectal cancer	104 (38%)
HCC	68 (25%)
Neuroendocrine tumor	45 (16%)
Cholangiocellular carcinoma	21 (8%)
Others	34 (13%)
Thrombus	
Segmental right portal vein	9
Lobar left portal vein	4
Segmental right portal vein plus lobar left portal vein	1
Tumor thrombosis, main portal vein	2
Tumor thrombosis, right hepatic vein	1
Portal hypertension	33
$\text{LSF}_{\text{MAA}}$ (%)	
Mean	5.73 (0.49–50.44)
Median	3.87 (4.60)
Number of cases > 20%	11
$\text{LSF}_{\text{Y-90}}$ (%)	
Mean	5.90 (0.27–39.02)
Median	4.13 (5.28)
Number of cases > 20%	7
$^{99\text{m}}\text{Tc}$ -based prediction of LMD (Gy)	
Mean	6.93 (0.17–89.03)
Median	3.52 (6.48)
Number of cases > 30 Gy	14
$^{90}\text{Y}$ PET-based left lung dose (Gy)	
Mean	1.59 (0.02–22.14)
Median	0.95 (1.16)
Number of cases > 12 Gy	3
Median total lung volume (mL)	1,713 (392–7,851)
Median left lung volume (mL)	733 (80–3,792)

Qualitative data are number; continuous data are mean and range or median and interquartile range.

**TABLE 2**  
Matrix of Statistical Significance of Differences Between Tumor Types in Terms of LSF<sub>Y-90</sub>

Type	LSF <sub>Y-90</sub>				
	Cholangiocellular carcinoma	Colorectal cancer	HCC	Neuroendocrine tumor	Others
Cholangiocellular carcinoma	—	0.5	0.5	0.06	0.5
Colorectal cancer		—	0.4	0.008*	0.5
HCC			—	0.01*	0.4
Neuroendocrine tumor				—	0.02*
Others					—

\*Statistically significant ( $P < 0.05$ ).

1,300 MBq. Details on this case were previously provided by Alsultan et al. (11).

Another subject, with an LMD<sub>Y-90</sub> of 18.4 Gy (LMD<sub>MAA</sub>, 29.1 Gy; LSF<sub>MAA</sub>, 19%), died of progressive disease 2 mo after treatment, before the evaluation scan could be done.

### DISCUSSION

The 30-Gy limit on maximum absorbed dose to the lungs for a single radioembolization treatment was based on clinical evidence from 2 seminal publications (4,5) that have strongly influenced the guidance on lung dose limits after radioembolization. This observational study showed that no patients with an LMD<sub>Y-90</sub> below 12 Gy developed any lung-dose-related side effects. Of the 14 patients who had an LMD<sub>MAA</sub> above 30 Gy, 2 developed radiation pneumonitis. However, the 12 other patients with an LMD<sub>MAA</sub> above 30 Gy did not develop any lung-dose-related side effects, stressing the limitation of using <sup>99m</sup>Tc-MAA planar scintigraphy in predicting <sup>90</sup>Y lung shunts.

Radiation pneumonitis is a rare but potentially fatal side effect of radioembolization. As summarized by Cremonesi et al. (19), there have been various reports of the lung-dose-related side effects of <sup>90</sup>Y radioembolization, in an attempt to improve insight on how to define the upper dose limit to the lungs. However, although they all used the same approach to computing the lung dose, namely multiplying the LSF<sub>MAA</sub> by the administered activity to estimate the LMD, different values for the lung dose above which radiation pneumonitis occurred were found (ranging between 10 and 56 Gy). In line with the 12 false-positive cases reported in this study (Fig. 3), Salem et al. (20) reported 58 patients treated with cumulative or single-treatment lung doses exceeding 30 Gy, based on LSF<sub>MAA</sub>-derived calculations, who did not develop any radiation pneumonitis or lung toxicity. These findings further underline how <sup>99m</sup>Tc particles overestimate the actual lung shunt. In contrast, Leung et al. (4) reported radiation pneumonitis in 3 patients with a predicted LMD lower than 30 Gy. However,

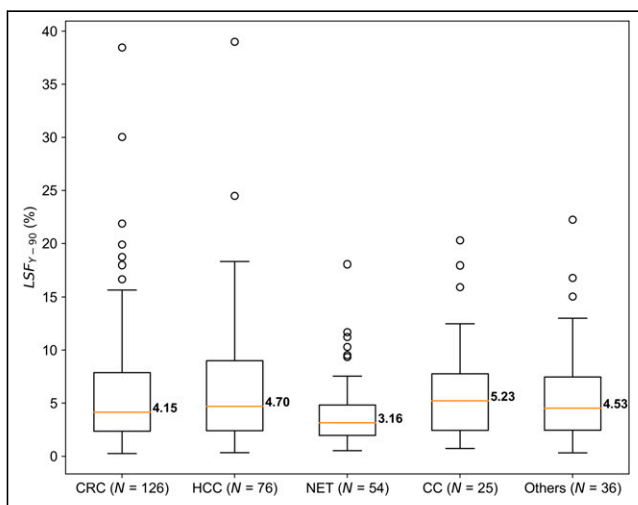


**FIGURE 2.** Box plots depicting LSF<sub>Y-90</sub>, together with corresponding median, divided by tumor type. Statistically significant difference was reported between neuroendocrine tumor patients and colorectal cancer patients ( $P = 0.008$ ), between neuroendocrine tumor and HCC patients ( $P = 0.010$ ), and between neuroendocrine tumor and patients in group “others” ( $P = 0.022$ ). CC = cholangiocellular carcinoma; CRC = colorectal cancer; NET = neuroendocrine tumor.

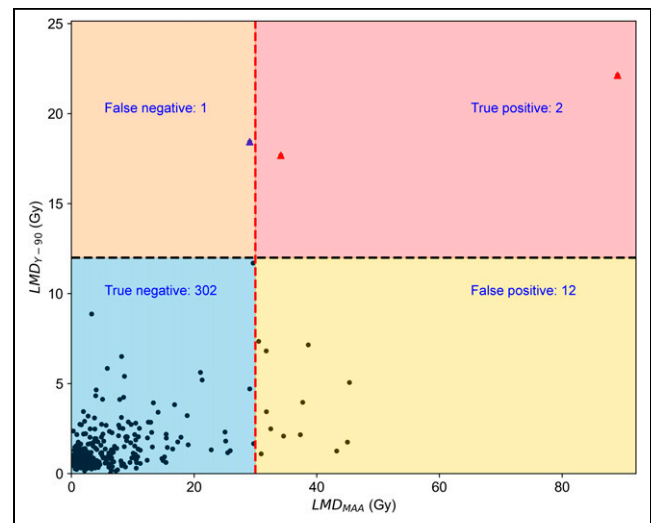


**FIGURE 3.** Distribution of LMD<sub>Y-90</sub> as function of corresponding LMD<sub>MAA</sub>. On the basis of limit of 30 Gy for estimate of absorbed radiation dose to lungs during pretreatment phase and 12 Gy for LMD<sub>Y-90</sub>, below which no radiation pneumonitis cases were reported, subjects were divided into 4 quadrants: true-positive, false-positive, true-negative, and false-negative. According to chosen limits, 12 false-positives were detected. True-positive (red triangles) corresponds to 2 patients who developed radiation pneumonitis, whereas false-negative (blue triangle) corresponds to patient who died of progressive disease before follow-up.

the absorbed doses taken from the literature were derived without including attenuation correction and thus should be rescaled by an average factor of 0.6 (21). For this reason, a straight comparison with the results of the current study is difficult. In addition, in this study,  $LMD_{Y-90}$  was computed on the posttreatment  $^{90}Y$  PET and considering only the left lung as representative of the lung volume. In this study, the same difficulties were found in determining a unique threshold for the  $^{99m}Tc$ -MAA-based LMD estimate to avoid radiation pneumonitis, confirming an issue well documented in the literature. As an example, in a multicenter study, Braat et al. (22) reported a patient with an  $LSF_{MAA}$  of 3% who developed radiation pneumonitis, whereas the patient with the highest  $LSF_{MAA}$ , 33%, did not develop radiation pneumonitis. These contradictory findings in the literature underline the limits of  $^{99m}Tc$ -MAA LSF, and consequently lung dose estimate, as predictive of  $^{90}Y$  distribution (9), stressing the need for a more reliable and robust method or particle. In recent years, some alternatives to  $^{99m}Tc$ -MAA have been suggested. Kunnen et al. (23) demonstrated in a phantom study that bremsstrahlung SPECT/CT, reconstructed with a Monte Carlo algorithm, can estimate the LSF for a  $^{90}Y$  pretreatment procedure using a theoretically safe  $^{90}Y$  activity of as low as 70 MBq.  $^{166}Ho$  scout microspheres (250 MBq; QuiremScout), already used as scout particles before  $^{166}Ho$  radioembolization, were proposed as a surrogate of  $^{90}Y$  to determine patients' eligibility, thanks to its imaging possibility (24).

Both patients who developed radiation pneumonitis in this study had HCC. Both cirrhosis and HCC have been associated with increased arteriovenous shunting into the lungs, potentially causing increased lung doses (25). However, significant differences were observed in  $LSF_{Y-90}$  only for HCC patients when compared with NET-diagnosed subjects (Fig. 2). In the subgroup of HCC patients only, the presence of either a thrombus or portal hypertension did not play a statistically significant role in  $LSF_{Y-90}$ , suggesting that these variables might be negligible when assessing the lung-dose-related side effects of  $^{90}Y$ . Conversely, Ward et al. (26), who reviewed 409 patients, reported a low but significant correlation between increased hepatopulmonary shunt fraction (measured using  $^{99m}Tc$ -MAA planar scintigraphy) and HCC, hepatic vein tumor thrombosis, and portal vein tumor thrombosis.

Several limitations apply to this study, apart from its retrospective and single-center nature. Considering the  $^{99m}Tc$ -based  $LMD_{MAA}$  computation, the main limitation is use of a surrogate model applying  $^{99m}Tc$ -MAA particles as an approximation to  $^{90}Y$  microsphere distribution. In addition, the lungs and liver were delineated on planar scintigraphy without an anatomic reference and assuming a fixed lung mass of 1 kg. Therefore, women, who have a smaller organ mass (27,28) than men but the same lung shunt, may have received a larger lung radiation dose for the same treatment activity. Like the  $^{90}Y$  PET-based  $LMD_{Y-90}$  computation, a constant value for lung density was used. However, as reported by Kappadath et al. (29), use of a constant value might be a limiting factor in an accurate estimate of  $LMD_{Y-90}$ . Although this study relied on the assumption of lung homogeneity, given that the lungs were not completely within the PET field of view for some datasets, the distribution of microspheres in vivo is heterogeneous (17). The gravitational dependence of alveolar and vascular pressures within the lung causes preferential distribution of blood flow and, in parallel, microspheres to the bases of the lung (30). In addition, microsphere irradiation is microscopically nonuniform (31). However, if radiation pneumonitis occurs, the assumption of a uniform distribution in the lung was visually

confirmed by the contrast-enhanced CT scan acquired during follow-up. Regardless, these limitations reflect the current protocols and treatment of patients. Moreover, radiation pneumonitis is a rare side effect of radioembolization, with just 2 cases among the 317 procedures in this study—a number of events too limited for any realistic statistical analysis.

Despite these limitations, a better predictive particle and a new lung dose limit are essential to improve the current general method of selecting patients, avoiding unjustified patient exclusion. Given the proven value of posttreatment  $^{90}Y$  PET/CT (20), more insight should be gained on the actual lung dose delivered than on the predicted one.

## CONCLUSION

This observational study showed that radiation pneumonitis did not occur among subjects with a left LMD below 12 Gy, defined on posttreatment  $^{90}Y$  PET/CT. A  $^{99m}Tc$ -MAA planar scintigraphy-based estimated cutoff of 30 Gy for lung dose is capricious and, once encountered in pretreatment imaging, should be evaluated with caution to prevent unjustified treatment exclusion.

## DISCLOSURE

Martina Stella is employed by the UMC Utrecht under a collaborative grant from the Dutch Research Council (NWO) between UMC Utrecht and Quirem Medical BV. Rob van Rooij and Hugo de Jong have acted as consultants for BTG/Boston Scientific. Arthur Braat has acted as a consultant for BTG/Boston Scientific and Terumo. Marnix Lam has acted as a consultant for BTG/Boston Scientific and Terumo and receives research support from BTG/Boston Scientific and Quirem Medical BV. The Department of Radiology and Nuclear Medicine of the UMC Utrecht receives royalties from Quirem Medical BV. No other potential conflict of interest relevant to this article was reported.

## ACKNOWLEDGMENTS

We thank the IT staff, in particular Marloes van Ijzendoorn, for help and support in providing anonymized data. We express gratitude to Sander Ebbens, who helped with the statistical analysis.

## KEY POINTS

**QUESTION:** What is the LMD below which radiation pneumonitis does not occur after  $^{90}Y$  radioembolization?

**PERTINENT FINDINGS:** This retrospective study showed that all subjects with an LMD below 12 Gy, measured on posttreatment  $^{90}Y$  PET/CT, did not develop radiation pneumonitis.

**IMPLICATIONS FOR PATIENT CARE:** Our findings suggest reconsideration of the current clinically used upper limit for LMD, 30 Gy.

## REFERENCES

1. Braat AJAT, Smits MLJ, Braat MNGJA, et al.  $^{90}Y$  hepatic radioembolization: an update on current practice and recent developments. *J Nucl Med*. 2015;56:1079–1087.
2. Salem R, Thurston KG. Radioembolization with  $^{90}Y$  microspheres: a state-of-the-art brachytherapy treatment for primary and secondary liver malignancies—part 1: technical and methodologic considerations. *J Vasc Interv Radiol*. 2006;17:1251–1278.

3. Peterson JL, Vallow LA, Johnson DW, et al. Complications after  $^{90}\text{Y}$  microsphere radioembolization for unresectable hepatic tumors: an evaluation of 112 patients. *Brachytherapy*. 2013;12:573–579.
4. Leung TWT, Lau WY, Ho SKW, et al. Radiation pneumonitis after selective internal radiation treatment with intraarterial  $^{90}\text{Y}$  yttrium-microspheres for inoperable hepatic tumors. *Int J Radiat Oncol Biol Phys*. 1995;33:919–924.
5. Ho S, Lau WY, Leung TWT, Chan M, Johnson PJ, Li AKC. Clinical evaluation of the partition model for estimating radiation doses from yttrium-90 microspheres in the treatment of hepatic cancer. *Eur J Nucl Med*. 1997;24:293–298.
6. Kappadath SC, Lopez BP, Salem R, Lam MGEH. Reassessment of the lung dose limits for radioembolization. *Nucl Med Commun*. 2021;42:1064–1075.
7. Lopez B, Mahvash A, Lam MGEH, Kappadath SC. Calculation of lung mean dose and quantification of error for  $^{90}\text{Y}$ -microsphere radioembolization using  $^{99\text{m}}\text{Tc}$ -MAA SPECT/CT and diagnostic chest CT. *Med Phys*. 2019;46:3929–3940.
8. Elschot M, Nijssen JFW, Lam MGEH, et al.  $^{99\text{m}}\text{Tc}$ -MAA overestimates the absorbed dose to the lungs in radioembolization: a quantitative evaluation in patients treated with  $^{166}\text{Ho}$ -microspheres. *Eur J Nucl Med Mol Imaging*. 2014;41:1965–1975.
9. Wondergem M, Smits MLJ, Elschot M, et al.  $^{99\text{m}}\text{Tc}$ -macroaggregated albumin poorly predicts the intrahepatic distribution of  $^{90}\text{Y}$  resin microspheres in hepatic radioembolization. *J Nucl Med*. 2013;54:1294–1301.
10. Alsultan AA, Smits MLJ, Barentsz MW, Braat AJAT, Lam MGEH. The value of yttrium-90 PET/CT after hepatic radioembolization: a pictorial essay. *Clin Transl Imaging*. 2019;7:303–312.
11. D'Arienzo M, Pimpinella M, Capogni M, et al. Phantom validation of quantitative Y-90 PET/CT-based dosimetry in liver radioembolization. *EJNMMI Res*. 2017;7:94.
12. Kunnen B, Beijst C, Lam MGEH, Viergever MA, de Jong HWAM. Comparison of the Biograph Vision and Biograph mCT for quantitative  $^{90}\text{Y}$  PET/CT imaging for radioembolisation. *EJNMMI Phys*. 2020;7:14.
13. Dittmann H, Kopp D, Kupferschlaeger J, et al. A prospective study of quantitative SPECT/CT for evaluation of lung shunt fraction before SIRT of liver tumors. *J Nucl Med*. 2018;59:1366–1372.
14. Hofmanninger J, Prayer F, Pan J, Röhrich S, Prosch H, Langs G. Automatic lung segmentation in routine imaging is primarily a data diversity problem, not a methodology problem. *Eur Radiol Exp*. 2020;4:50.
15. Rhodes CG, Wollmer P, Fazio F, Jones T. Quantitative measurement of regional extravascular lung density using positron emission and transmission tomography. *J Comput Assist Tomogr*. 1981;5:783–791.
16. Pasciak AS, Bourgeois AC, Bradley YC. A comparison of techniques for  $^{90}\text{Y}$  PET/CT image-based dosimetry following radioembolization with resin microspheres. *Front Oncol*. 2014;4:121.
17. Bastiaannet R, Kappadath SC, Kunnen B, Braat AJAT, Lam MGEH, de Jong HWAM. The physics of radioembolization. *EJNMMI Phys*. 2018;5:22.
18. Levillain H, Bagni O, Deroose CM, et al. International recommendations for personalised selective internal radiation therapy of primary and metastatic liver diseases with yttrium-90 resin microspheres. *Eur J Nucl Med Mol Imaging*. 2021;48:1570–1584.
19. Cremonesi M, Chiesa C, Strigari L, et al. Radioembolization of hepatic lesions from a radiobiology and dosimetric perspective. *Front Oncol*. 2014;4:210.
20. Salem R, Parikh P, Atassi B, et al. Incidence of radiation pneumonitis after hepatic intra-arterial radiotherapy with yttrium-90 microspheres assuming uniform lung distribution. *Am J Clin Oncol*. 2008;31:431–438.
21. Chiesa C, Maccauro M, Romito R, et al. Need, feasibility and convenience of dosimetric treatment planning in liver selective internal radiation therapy with  $^{90}\text{Y}$  microspheres: the experience of the National Tumor Institute of Milan. *Q J Nucl Med Mol Imaging*. 2011;55:168–197.
22. Braat AJAT, Kappadath SC, Ahmadzadehfard H, et al. Radioembolization with  $^{90}\text{Y}$  resin microspheres of neuroendocrine liver metastases: international multicenter study on efficacy and toxicity. *Cardiovasc Intervent Radiol*. 2019;42:413–425.
23. Kunnen B, van der Velden S, Bastiaannet R, Lam MGEH, Viergever MA, de Jong HWAM. Radioembolization lung shunt estimation based on a  $^{90}\text{Y}$  pretreatment procedure: a phantom study. *Med Phys*. 2018;45:4744–4753.
24. Prince JF, van Rooij R, Bol GH, de Jong HWAM, van den Bosch MAAJ, Lam MGEH. Safety of a scout dose preceding hepatic radioembolization with  $^{166}\text{Ho}$  microspheres. *J Nucl Med*. 2015;56:817–823.
25. Kallini JR, Gabr A, Salem R, Lewandowski RJ. Transarterial radioembolization with yttrium-90 for the treatment of hepatocellular carcinoma. *Adv Ther*. 2016;33:699–714.
26. Ward TJ, Tamrazi A, Lam MGEH, et al. Management of high hepatopulmonary shunting in patients undergoing hepatic radioembolization. *J Vasc Interv Radiol*. 2015;26:1751–1760.
27. Molina DK, DiMaio VJM. Normal organ weights in women: part II—the brain, lungs, liver, spleen, and kidneys. *Am J Forensic Med Pathol*. 2015;36:182–187.
28. Molina DK, DiMaio VJM. Normal organ weights in men: part II—the brain, lungs, liver, spleen, and kidneys. *Am J Forensic Med Pathol*. 2012;33:368–372.
29. Kappadath SC, Lopez BP, Salem R, Lam MG. Lung shunt and lung dose calculation methods for radioembolization treatment planning. *Q J Nucl Med Mol Imaging*. 2021;65:32–42.
30. Armstrong J, Raben A, Zelefsky M, et al. Promising survival with three-dimensional conformal radiation therapy for non-small cell lung cancer. *Radiother Oncol*. 1997;44:17–22.
31. Giammarile F, Bodei L, Chiesa C, et al. EANM procedure guideline for the treatment of liver cancer and liver metastases with intra-arterial radioactive compounds. *Eur J Nucl Med Mol Imaging*. 2011;38:1393–1406.